Euler Monte Carlo calculations for liquid ^{4}He and ^{3}He

Saverio Moroni
Istituto Nazionale di Fisica della Materia, Laboratorio FORUM, Scuola Normale Superiore, Piazza dei Cavalieri 7, I–56126 Pisa, Italy

Stefano Fantoni
Interdisciplinary Laboratory, Scuola Internazionale Superiore di Studi Avanzati, Via Beirut 2/4, I-34014, Trieste, Italy and International Centre for Theoretical Physics, I-34014, Trieste, Italy

Gaetano Senatore
Dipartimento di Fisica Teorica, Università di Trieste, Strada Costiera 11, I-34014 Trieste, Italy
(Received 12 April 1995; revised manuscript received 21 June 1995)

We present an optimization procedure for Monte Carlo variational calculations and illustrate it by optimizing pair and triplet correlations in the ground-state wave functions of liquid ^{4}He and ^{3}He. We use the optimized trial functions, with a partially optimized backflow for ^{3}He, to perform extensive diffusion Monte Carlo simulations that yield accurate results for the equation of state and structural properties of both liquids. The agreement with experiments, which is excellent for ^{4}He, somewhat deteriorates in going to ^{3}He, due to the use of the fixed-node approximation. The remaining appreciable discrepancies between the results of variational and diffusion Monte Carlo unambiguously point to the increasing importance of n-body correlations, with $n>3$, as the density is increased.

I. INTRODUCTION

The optimization of variational wave functions of quantum liquids is a long-standing problem, which has been attacked for many years with hypernetted-chain (HNC, FHNC) theories[1–4] and, more recently, within the variational Monte Carlo (VMC) method.[5,6] Most calculations using HNC theories have been mainly devoted to the optimization of the Jastrow pair factor $f_2(r)$ of the trial wave function. Thus it has been possible to determine the long-range behavior[7] of $f_2(r)$ and, moreover, the optimized $f_2(r)$ obtained by solving numerically the HNC Euler equations has provided improved energy upper bounds with respect to parametrized $f_2(r)$, like the MacMillan ansatz. However, the elementary diagrams entering the HNC cannot be summed up in any known closed form and can be accounted for only in approximate manners.[8,2–4] Hence, also the HNC Euler equations are intrinsically approximated. Moreover, if the trial wave function contains higher-order terms in the Feenberg expansion,[9,10] like triplets, the corresponding Euler equations become increasingly involved and difficult to solve numerically.[11,2]

Recently Vitiello and Schmidt[5] have proposed an optimization procedure for the Jastrow correlation factor $f_2(r)$ of liquid ^{4}He, which is based on the variational Monte Carlo method. In their calculation, $f_2(r)$ is built up using the first few eigenfunctions of a suitable Schrödinger-like equation,[12] which is quite effective in keeping low the number of basis components in the expansion of $f_2(r)$.

Triplet correlations play an important role in the physics of both liquid ^{4}He and ^{3}He, as Jastrow models provide poor upper bounds of the energy per particle $E(\rho)$. For instance, at the experimental equilibrium density ρ_{eq}, Jastrow correlations overestimate the total energy by about 1 K for both ^{4}He and ^{3}He with respect to Green function Monte Carlo[13] (GFMC) or diffusion Monte Carlo[14] (DMC) solutions, which are known to provide virtually exact results for bosons[6] and variational upper bounds to the total energy of fermions, within the fixed-node approximation.[15] The inclusion of triplet correlations is essential in bringing the equilibrium density ρ_{eq} close to the experimental values and considerably improves the equations of state of the two liquids. However, non-negligible discrepancies with GFMC or DMC solutions still remain. It is one of the goals of the present study to establish whether such discrepancies are due to the use of nonoptimized triplets or to the need of n-body correlations, with $n>3$.

In this paper we implement a basis set method similar to that of Ref. 5 in order to optimize not only the Jastrow pair function, but also the triplet correlation functions. By combining the reweighting method[16] for variance minimization[17] with a technique which makes use of the derivatives of the local energy with respect to the expansion parameters,[18,19] it is possible to deal with a number of basis components which is large enough that the whole procedure is equivalent to solve the Euler equations for the pair and the triplet correlation functions.

Using trial wave functions with optimized pair and triplet correlations, we have calculated the equation of state for both ^{4}He and ^{3}He. The energy upper bounds are lower than those obtained from trial functions used in previous variational calculations. The improvement becomes significant in the high-density regime. Variational optimization is important, not only for the understanding of correlations, but also for Green function Monte Carlo or diffusion Monte Carlo calculations. Particularly, when calculating quantities other than energy per particle $E(\rho)$, like for instance the pair distribution func-

0163-1829/95/52(18)/13547(12)/$06.00

tion $g(r)$ or the kinetic energy, a good trial wave function is very much needed to reduce systematic errors in the extrapolated estimates.[6] Using these optimized variational wave functions for importance sampling, we could perform fixed node DMC calculations at an unprecedented accuracy. The comparison between variational and DMC results shows that n-body correlations with $n>3$ definitely play an important role, particularly at high densities, as also indicated by recent VMC calculations carried out by using Shadow wave functions.[20] A preliminary account of our results has been given elsewhere.[21]

The plan of the paper is as follows. The VMC method is discussed in Sec. II and the Euler optimization procedure in Sec. III. The DMC calculations are discussed in Sec. IV and the results obtained for liquid ^{4}He and ^{3}He are presented in Sec. V. The last section is devoted to conclusions.

II. VARIATIONAL MONTE CARLO METHOD

It is believed that the Hamiltonian

$$H=-\frac{\hbar^2}{2m}\sum_{i=1}^{N}\Delta_i+\sum_{i<j=1}^{N}v(r_{ij}), \tag{1}$$

where $v(r)$ is the HFDHE2 potential of Aziz *et al.*[22,13] provides a realistic description of both the Bose and the Fermi liquid helium, at relatively low pressure.

The expectation value of the Hamiltonian $\langle H\rangle$ is computed by generating a set $\{R\}$ of M configurations R_i sampled from the probability

$$P(R)=\frac{|\Psi_0(R)|^2}{\int dR'|\Psi_0(R')|^2}, \tag{2}$$

by means of a generalized Metropolis algorithm,[23] and averaging the *local energy* $E_L(R)$,

$$\langle H\rangle\simeq\frac{1}{M}\sum_i E_L(R_i), \tag{3}$$

$$E_L(R)=\frac{1}{\Psi_0(R)}H\Psi_0(R)=V(R)+\frac{1}{\Psi_0(R)}T(R)\Psi_0(R)$$
$$=\sum_{i<j=1}^{N}v(r_{ij})+\frac{\hbar^2}{2m}\sum_i[h_i(R)-\mathbf{g}_i(R)\cdot\mathbf{g}_i(R)]; \tag{4}$$

here

$$h_i(R)=-\Delta_i\ln\Psi_0(R), \tag{5}$$

$$\mathbf{g}_i(R)=-\nabla_i\ln\Psi_0(R), \tag{6}$$

and R denotes the coordinates $\mathbf{r}_1,\ldots,\mathbf{r}_N$ of all particles.

We have used trial functions containing Jastrow and triplet correlations for the Bose case,[24] and Jastrow, triplet, and backflow correlations for the Fermi system,[25] namely,

$$\Psi_0=F_3\Phi, \tag{7}$$

where

$$F_3=\exp\left[-\frac{1}{2}\sum_{i<j=1}^{N}u_2(r_{ij})-\frac{1}{2}\sum_{i<j<k=1}^{N}u_3(i,j,k)\right], \tag{8}$$

with $f_2(r)=\exp[-u_2(r)/2]$ the Jastrow correlation function. Here, Φ is equal to a constant for ^{4}He and a product of the spin-up and spin-down Slater determinants of plane waves with backflow correlations for ^{3}He:

$$\Phi_{^4\mathrm{He}}=1, \tag{9}$$

$$\Phi_{^3\mathrm{He}}=\phi_B(\uparrow)\phi_B(\downarrow), \tag{10}$$

where $\phi_B(\alpha)$ $(\alpha=\uparrow,\downarrow)$ are given by

$$\phi_B(\alpha)=Det_{ij}\left\{\exp\left[i\mathbf{k}_i\cdot\left(\mathbf{r}_j+\sum_{k\neq j}^{N}\eta(r_{kj})\mathbf{r}_{kj}\right)\right]\right\}; \tag{11}$$

the wave vectors $\mathbf{k}_i$ span the $N/2$ allowed momenta of the Fermi sea and j ranges from 1 to $N/2$ for $\alpha=\uparrow$ and $N/2+1$ to N for $\alpha=\downarrow$, whereas the sum over k is extended to all the particles. The backflow correlation is taken in the form[25]

$$\eta(r)=\lambda_B\exp\left[-\left(\frac{r-r_B}{\omega_B}\right)^2\right]\left(\frac{2r-L}{L}\right)^3, \tag{12}$$

where λ_B, r_B, and ω_B are variational parameters, and L is the side of the simulation box. The evaluation of the determinant and its derivatives entering the kinetic energy is the most time-consuming part of the algorithm. It is performed as explained in Ref. 26.

The pair and triplet pseudopotentials in Eq. (8) have been taken as linear superpositions of suitable basis functions $\chi_m(r)$, to be specified in Sec. V,

$$u_2(r_{ij})=u_2^0(r_{ij})+\sum_m a_m\chi_m(r_{ij}), \tag{13}$$

$$u_3(i,j,k)=u_3^0(i,j,k)$$
$$+\sum_{\mathrm{cyc}}\sum_{m,n,\ell}b_{mn}^{\ell}\chi_m(r_{ij})\chi_n(r_{ik})P_\ell(\hat{\mathbf{r}}_{ij}\cdot\hat{\mathbf{r}}_{ik}), \tag{14}$$

where the *Feynman* ansatz u_3^0, given by

$$u_3^0(i,j,k)=\sum_{\mathrm{cyc}}\xi^0(r_{ij})\xi^0(r_{ik})P_1(\hat{\mathbf{r}}_{ij}\cdot\hat{\mathbf{r}}_{ik}), \tag{15}$$

is believed to provide a realistic representation of triplet correlations. In the above equations, P_ℓ are Legendre polynomials. The matrices b_{mn}^{ℓ} must be symmetrical in m,n, and "cyc" denotes a sum over cyclic permutations of $\{ijk\}$. The ansatz $b_{mn}^{\ell}=b_m^{\ell}b_n^{\ell}$ restricts the class of triplet correlation functions to those of the *factorized* form

$$u_3^F(i,j,k)=\sum_{\ell}\sum_{\mathrm{cyc}}\xi_\ell(r_{ij})\xi_\ell(r_{ik})P_\ell(\hat{\mathbf{r}}_{ij}\cdot\hat{\mathbf{r}}_{ik}), \tag{16}$$

where $\xi_\ell(r)=\Sigma_m b_m\chi_m(r)$. This form implies a much smaller number of variational parameters to be considered with respect to that of Eq. (11), but has a quadratic dependence on the expansion parameters b_m^{ℓ}. We have optimized

u_3^F by retaining only the $\ell=0,1$ components, which are known to be the most important.[3] The general form of u_3 of Eq. (11) has also been optimized, retaining the $\ell=0,1$ component only. Higher order components, in fact, have been shown to be negligible.[3]

The main problem is to optimize the trial function Ψ_0, minimizing $\langle H\rangle$, or its variance or a combination of them, under variation of the parameters of the backflow correlation and the expansion coefficients a_m and b_{mn}^{ℓ} of the pair and the triplet correlation functions. It will be shown in the next section that the optimization of u_2 and u_3 relies on the feature that $\ln F_3$ is linear (or quadratic) in the expansion coefficients. This feature does not hold for the backflow correlation, which, for this reason, we have not attempted to fully optimize.

III. OPTIMIZATION METHOD

The Euler Monte Carlo (EMC) procedure that we propose in this paper is based on the minimization of a combination σ^2 of the energy expectation value and its variance,[17] using the reweighting method[16] and the feature that $\ln\Psi_0$ is linear (or quadratic) in the variational parameters.[18,19] We pose no restrictions on the functional form of the pair and triplet correlations, pushing the expansions of Eqs. (13) and (14) to convergence (within a threshold given by statistical accuracy). Thus we solving the variational problem for $\sigma^2([u_2],[u_3])$, which is equivalent to solving the Euler equations

$$\frac{\delta\sigma^2}{\delta u_n(\mathbf{r}_1,\ldots,\mathbf{r}_n)}=0 \quad (n=2,3), \tag{17}$$

for the pair and triplet correlations. Note, however, that such Euler equations do not enter explicitly the Monte Carlo optimization scheme.

A. Variance minimization

It has become widespread practice to optimize a highly parametrized wave function by minimizing with respect to the variational parameters the positive quantity

$$\sigma^2=\frac{1}{M}\sum_i [E_L(R_i)-E_0]^2, \tag{18}$$

rather than the variational energy itself.[17] If E_0 is the average local energy, σ^2 is its variance.

Variance minimization has several advantages. Since Eq. (18) is a sum of squares, it can be minimized by a very efficient algorithm such as that of Levenberg and Marquardt.[27] However, in the present work this is only a marginal bonus because, for a given sample $\{R_i\}$ used in the evaluation of σ^2, we can move at basically no cost through the parameter space (see below) and the efficiency of the minimization algorithm is not crucial. More importantly, variance minimization requires a much smaller number of configurations than energy minimization. In fact, consider the ideal limit of a wave function that recovers the exact ground state for a given choice of a finite number N_p of variational parameters. It is evident, from Eq. (18) and the property that the variance be zero for the exact wave function,[17] that N_p configurations provide N_p conditions, which in general will be sufficient to fix all the parameters. Even though the ideal limit is never attained, the better is the wave function, the smaller the number of needed configurations. Finally, the only way the variance can be small is that the wave function be accurate in all the configuration space, making the local energy $E_L(R)$ smooth (the local energy is obviously constant for the exact wave function). Energy minimization, on the other hand, may be biased by configurations where the local energy is too low: This gives a stronger dependence on the finite sample $\{R_i\}$ used in Eq. (18), and occasionally may produce less accurate variational parameters.

Since the form of the trial wave function is not exact, there is no guarantee that a set of parameters which minimizes the variance so does for the energy as well. We intentionally shift E_0 slightly below the average local energy, to give some weight to the variational energy in the quantity to be minimized.[17] The amount of the shift is chosen to be ~ 1 K because, in some test cases, this choice produced a better variational energy with no significant increase of the variance.

B. Reweighting method

The reweighting technique[16] is adopted to efficiently minimize σ^2 with respect to the variational parameters. It consists of using the set of configurations $\{R_i\}$, obtained from the distribution $|\Psi_0|^2$, to estimate $(\sigma^2)'$ corresponding to a trial wave function Ψ_0' which is not *too different* from Ψ_0. This allows one to evaluate the difference $\sigma^2-(\sigma^2)'$ much more accurately than the quantity σ^2 itself. An independent sampling from $|\Psi_0'|^2$ would introduce large fluctuations in the (often small) difference $\sigma^2-(\sigma^2)'$.

Let us suppose that $\{R_i\}$ is a set of configurations drawn from $|\Psi_0|^2$. The estimate of $(\sigma^2)'$ is given by

$$(\sigma^2)'=\frac{\Sigma_i[E_L'(R_i)-E_0]^2 w(R_i)}{\Sigma_i w(R_i)}, \tag{19}$$

where the weights are given by

$$w(R)=\frac{|\Psi_0'(R)|^2}{|\Psi_0(R)|^2}=\exp\{2[l(R)-l'(R)]\}, \tag{20}$$

$$l(r)=-\ln\Psi_0(R), \tag{21}$$

and the local energy is given by

$$E_L'(R)=\frac{1}{\Psi_0'}H\Psi_0'=V(R)+\frac{\hbar^2}{2m}\sum_i [h_i'(R)-\mathbf{g}_i'(R)\cdot\mathbf{g}_i'(R)]. \tag{22}$$

We use a few thousand configurations in the sum (19) to optimize some tens of variational parameters (detailed values depend on the form of the wave function). New configurations are generated with the optimized parameters and the procedure is iterated until the energy and its variance converge within statistical errors. The rate of convergence of the reweighting procedure at any given density ρ depends upon the starting trial wave function Ψ_0. If we keep the optimized trial function, obtained at a density ρ_0 close to ρ, as starting

Ψ_0, two to three iterations are sufficient to reach convergence. However, even starting from a poor trial function such as a pure Jastrow form does not require more than ~ 10 iterations. Various tests, done starting from different initial values of the parameters, using different basis sets, and keeping iterate after convergence, indicate that the final energies are reliable to within 0.01 K.

C. Linearity of $\ln\Psi_0$ on the variational parameters

The reweighting technique is particularly efficient in the optimization procedure when $\ln\Psi_0$ is linear in the variational parameters.[18,19] According to Eqs. (13) and (14), $\ln\Psi_0$ is linear in the expansion coefficients a_m and $b_{mn}^{\not}$,

$$l(R)=l^0(R)+\sum_\alpha [a_\alpha l_2^\alpha(R)+b_\alpha l_3^\alpha(R)], \tag{23}$$

where, for brevity, we have used a single index α in the coefficients b and quantities l_3, which actually depend upon three indices $(m_\alpha,n_\alpha,\not_\alpha)$. The expressions of l^0, l_2, and l_3 are given by

$$l^0(R)=-\frac{1}{2}\left[\sum_{i<j=1}^{N} u_2^0(r_{ij})+\sum_{i<j<k=1}^{N} u_3^0(i,j,k)\right] \tag{24}$$

and

$$l_2^\alpha(R)=-\frac{1}{2}\sum_{i<j=1}^{N}\chi_\alpha(r_{ij}), \tag{25}$$

$$l_3^\alpha(R)=-\frac{1}{2}\sum_{i<j<k=1}^{N}\sum_{\text{cyc}}\chi_{m_\alpha}(r_{ij})\chi_{n_\alpha}(r_{ik})P_{\not_\alpha}(\hat r_{ij}\cdot\hat r_{ik}). \tag{26}$$

Similarly the functions $h_i(R)$ and $\mathbf{g}_i(R)$ are linear in the expansion coefficients. The expressions of $h_i^0(R)$, $h_{2i}^\alpha(R)$, $h_{3i}^\alpha(R)$ and of $\mathbf{g}_i^0(R)$, $\mathbf{g}_{2i}^\alpha(R)$, $\mathbf{g}_{3i}^\alpha(R)$ are obtained by acting on $l^0(R)$, $l_2^\alpha(R)$, $l_3^\alpha(R)$ with $-\Delta_i$ and $-\nabla_i$, respectively.

Inserting the expansions of $h_i(R)$ and $\mathbf{g}_i(R)$ into Eq. (4) one easily finds an expansion for the kinetic energy T which is quadratic in the expansion coefficients:

$$\begin{aligned}T(R)=T^0(R)&+\sum_\alpha [T_2^\alpha(R)a_\alpha+T_3^\alpha(R)b_\alpha]\\&+\sum_{\alpha,\alpha'}(T_{22}^{\alpha,\alpha'}a_\alpha a_{\alpha'}+T_{23}^{\alpha,\alpha'}a_\alpha b_{\alpha'}+T_{32}^{\alpha,\alpha'}b_\alpha a_{\alpha'}\\&+T_{33}^{\alpha,\alpha'}b_\alpha b_{\alpha'}),\end{aligned} \tag{27}$$

where

$$T^0(R)=\frac{\hbar^2}{2m}\sum_i [h_i^0(R)-\mathbf{g}_i^0(R)\cdot\mathbf{g}_i^0(R)], \tag{28}$$

$$T_\mu^\alpha(R)=\frac{\hbar^2}{2m}\sum_i [h_{\mu i}^\alpha(R)-2\mathbf{g}_{\mu i}^\alpha(R)\cdot\mathbf{g}_{\mu i}^0(R)], \tag{29}$$

$$T_{\mu\nu}^{\alpha,\alpha'}(R)=-\frac{\hbar^2}{2m}\sum_i \mathbf{g}_{\mu i}^\alpha(R)\cdot\mathbf{g}_{\nu i}^{\alpha'}(R), \tag{30}$$

with $\mu=2,3$ and $\nu=2,3$. The knowledge of l^α, as well as of the kinetic energy terms T^α and $T^{\alpha\alpha'}$ for any configuration R_i, allows us to compute the weights and the local energy in Eq. (19) for any choice of a_m and $b_{mn}^{\not}$ by the expansions (23) and (27). The expensive evaluation of the terms l^α, $\mathbf{g}_i^\alpha$, h_i^α has to be done only once, and the number of evaluations of σ^2 required by the minimization routine has little effect on the computational load.

The general form (14) of the triplet pseudopotential is extremely inefficient in the actual simulation because it requires explicit evaluation of each term m,n in the sum (14). Its use could only be justified by significant improvements over the factorized form, which turns out not to be the case.

The factorized form (16), on the other hand, is quadratic in the variational parameters, and the kinetic energy is quartic. This case can be treated by straightforward generalization of Eqs. (22)–(29). The scaling of the optimization algorithm with the number of variational parameters becomes quite unfavorable (fourth power), due to the derivatives to be added in expansion (27). However, the computational cost is still moderate for the number of basis functions we use (a typical optimization for ^{3}He requires a few hours on an IBM risc 6000/550 workstation, mostly devoted to generating the configurations $\{R_i\}$).

IV. DIFFUSION MONTE CARLO CALCULATIONS

Diffusion Monte Carlo[14,28] is a stochastic solution of the (bosonic) imaginary time Schrödinger equation

$$-\frac{\partial\Phi(R,t)}{\partial t}=-\frac{\hbar^2}{2M}\nabla^2\Phi(R,t)+V\Phi(R,t). \tag{31}$$

Since $\Phi(t\to\infty)=\Phi_0$, the lowest-energy eigenstate of the Hamiltonian not orthogonal to $\Phi(t=0)$, DMC gives information on the *exact* ground state of the system. The solution is obtained in principle by simulating the imaginary time Schrödinger equation (31) as a diffusion equation for the (positive) density $\Phi(R,t)$.

In practice, for reasons of computational efficiency, one has to introduce *importance sampling*. By multiplying Eq. (31) by a known trial function Ψ_0 and rearranging terms, one gets a new diffusion equation for the density $f(R,t)=\Psi_0\Phi(R,t)$:

$$\begin{aligned}-\frac{\partial f(R,t)}{\partial t}=&-\frac{\hbar^2}{2M}\nabla^2 f(R,t)+\frac{\hbar^2}{2M}\nabla\cdot[\mathbf{F}(R)f(R,t)]\\&+[E_L(R)-E_T]f(R,t),\end{aligned} \tag{32}$$

where $\mathbf{F}(R)=2\nabla\Psi_0(R)/\Psi_0(R)$, $E_L(R)$ is the local energy defined in Eq. (4), and E_T is a normalization constant. This new diffusion equation has a drift term $\nabla\cdot(\mathbf{F}f)$ which drives the density towards regions where Ψ_0 is large. Moreover, the branching term $(E_L-E_T)f$ contains the local energy, which is smooth for a good wave function, instead of the potential V which has large fluctuations. Both these facts improve the efficiency because in the actual calculation one has a discrete representation and a finite sampling of the density f, and hence wants to sample preferably important regions and avoid large fluctuations.

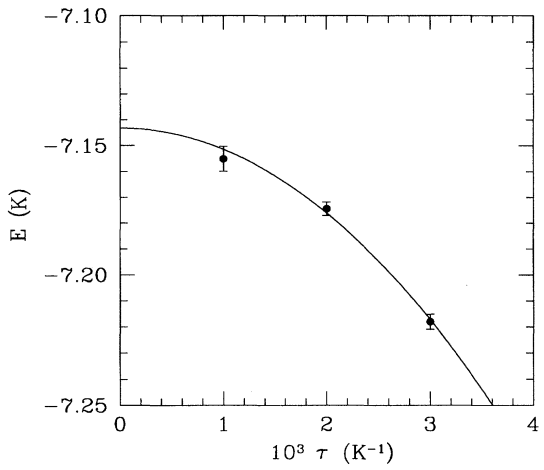

FIG. 1. Extrapolation at $\tau=0$ for the total energy E, in ^{4}He, at the experimental equilibrium density $\rho_{eq}=0.021\ 86\ \text{Å}^{-3}$.

Since Eqs. (32) and (31) are formally equivalent, the density $f(R,t)$ will converge to $\Psi_0\Phi_0$ at large t. The configurations $\{R_i\}$ generated in the Monte Carlo simulation are asymptotically sampled from $\Psi_0\Phi_0$, and can be used to evaluate the *mixed estimator*[6]

$$O_{\text{mix}}=\frac{\langle\Psi_0|\hat{O}|\Phi_0\rangle}{\langle\Psi_0|\Phi_0\rangle}\simeq\frac{1}{\mathcal{N}}\sum_{i=1}^{\mathcal{N}}\frac{\hat{O}\Psi_0(R_i)}{\Psi_0(R_i)} \tag{33}$$

of an operator $\hat{O}$. Only for operators which commute with the Hamiltonian will the mixed estimator coincide with the ground-state expectation value $\langle\Phi_0|\hat{O}|\Phi_0\rangle/\langle\Phi_0|\Phi_0\rangle$. For other operators, the bias in the mixed estimator is first order in δ, where $|\Phi_0\rangle=|\Psi_0\rangle+\delta|\Psi\rangle$. One can improve by computing the *extrapolated* estimator $O_{\text{ext}}=2O_{\text{mix}}-\langle\Psi_0|\hat{O}|\Psi_0\rangle/\langle\Psi_0|\Psi_0\rangle$. The bias in the extrapolated estimator is second order in δ. Methods to compute unbiased ground-state expectation values have been proposed;[29] however, they introduce large statistical errors, and in this paper we will use the extrapolated estimator.

In the actual simulation one evolves a discrete representation of the density $f(r,t)$ using a finite time step τ and an approximation for the Green function of the differential equation (32) which is only exact in the limit $\tau\to0$. This introduces a time step error which can be extrapolated out by repeating the simulation with various time steps. All the energies calculated in this work are extrapolated to $\tau=0$. A typical extrapolation is shown in Fig. 1. For the structural properties, on the other hand, the statistical noise was larger than the time step bias, and we report results for a fixed τ. The time step error can be avoided altogether by using the Green function Monte Carlo method.[6]

An exact practical algorithm for a general many-fermion problem is not known. For ^{3}He, we resort to the *fixed node approximation*,[15] which assumes that the ground state has the same nodal structure as the trial function. Then the density $f=\Phi_0\Psi_0$ is positive and can be sampled by the method outlined above. In practice one restricts the diffusion process not to cross the nodes of the trial function. The fixed node approximation has variational character, and gives the best energy upper bound consistent with the nodal structure of the trial function.

V. VARIATIONAL AND DMC RESULTS

In the variational calculations, the functions $u_2^0(r)$ and $\xi^0(r)$ in Eqs. (13) and (15) have been taken of the form

$$u_2^0(r)=\left(\frac{b}{r}\right)^5, \tag{34}$$

$$\xi^0(r)=a_t\exp\left[-\left(\frac{r-r_t}{w_t}\right)^2\right], \tag{35}$$

with $b=3.04$ Å, $a_t=0.0827$ Å^{-1}, $r_t=2.04$ Å, and $w_t=1.05$ Å for ^{4}He, and $b=2.94$ Å, $a_t=0$ for ^{3}He. The results reported in this paper have been obtained with the following basis functions:

$$\chi_m(r)=\left[1-\cos\left(\frac{2\pi m}{L-2r_c}(r-L/2)\right)\right]r^n \quad (r>r_c),$$
$$=r^n \quad (r<r_c), \tag{36}$$

where L is the side of the simulation box. Variational freedom is freezed for $r<r_c=1.75$, roughly corresponding to the range of interparticle distances which is never sampled by MC configurations, to avoid instabilities in the optimization procedure. The exponent n is taken equal to -5 in the expansion of u_2 and equal to ℓ in the ℓ component of u_3.

The choice of the basis functions is not really crucial, provided one takes into account the gross features of the function be optimized. In the present case, for instance, the choice of n in the expansion of u_2 sets the basis functions on a roughly appropriate scale. We have obtained equivalent results with a similar number of basis functions using Gaussians instead of cosines in Eq. (36). Most of the present results are obtained with 20 and 14 basis functions in the expansion of u_2 and u_3^F. Convergence has been verified including up to 30 and 20 basis functions, respectively. In all cases the parameters in the pair and triplet correlations are optimized simultaneously.

All simulations presented in this work have been done with 64 atoms of ^{4}He or 54 atoms of ^{3}He in a cubic box with periodic boundary conditions. To enforce periodicity the pair potential $v(r)$ was smoothly cutoff at $r_c=L/2$. We actually used $v'(r)\equiv v(r)-\Delta v(r)$,

$$v'=v(r)+v(L-r)-2v(L/2) \quad (r<r_c) \tag{37}$$

$$=0 \quad (r>r_c). \tag{38}$$

A correction $\Delta V=(1/2)\rho\int g(r)\Delta v(r)d\mathbf{r}$ was then added to the computed potential energy, where the pair correlation function $g(r)$ comes from the simulation and is taken equal to 1 for $r>L/2$. The functions u_2 and u_3 were modified according to the same prescription as for $v(r)$. In fact it has been shown[7] that a long-range term $\sim r^{-2}$ in the two-body pseudopotential u_2 would give the correct linear behavior of the structure factor $S(q)$ at small q. However, such a long-range term has an exceedingly small effect on the total

energy[30] and therefore we did not include it explicitly in our wave function or try to detect it in the optimized u_2.

Since we are mainly interested in the optimization of triplets, which are very short range, we did not perform a detailed study of the size dependence. However, we optimized the two-body correlation for ^{4}He at equilibrium density using either 64 or 108 atoms. We found that no further structure appears in the extra range of interparticle distances accessible with the larger simulation cell [i.e., $f_2(r)=1$ within statistical error for 7 Å$\leq r \leq$8.3 Å]. Also the optimized two-body correlations for $N=64$ and $N=108$ do not differ by a statistically significant amount, and yield the same total and kinetic energies. This justifies the simulation of relatively small systems for the purpose of energy or variance minimization with respect to the pair correlation.

Figure 2 shows the McMillan pair function $\exp[-u_2^0(r)/2]$ (dotted line) together with various optimized forms, for ^{4}He at equilibrium density. The dashed line corresponds to the optimal Jastrow wave function. It is larger than the McMillan function for $r \lesssim 4$ Å, and has a structure between $r=4$ and $r=6$, which may be attributed to a mimicking of three-body effects by the two-body correlation.[5] The solid line in Fig. 2 shows the optimized pair function for a wave function which also includes triplet correlations. As noted previously,[5,21] explicit inclusion of three-body terms reduces the structure between $r=4$ Å and $r=6$ Å.

For the case of the triplet correlation, we have first optimized u_3^F with the component $\ell=1$ only, keeping $b_{mn}^{\ell=1}=b_m^1 b_n^1$ [case JTF(1)]. The optimized $\xi_1(r)$ for ^{4}He at equilibrium density is shown in Fig. 2. It decreases more sharply than the parametrized form of Ref. 24 for $r\sim\sigma=2.556$ Å. The density dependence of the optimal $\xi_1(r)$ is very weak, and cannot be resolved, in the density range 0.019 64–0.026 22 Å^{-3}, within the accuracy of the present calculation. With respect to a wave function containing a parametrized Feynman form u_3^0 of the triplet[24] and an optimized u_2, the optimization of $\xi_1(r)$ lowers the variational energy of ^{4}He at equilibrium density by $\sim$0.04 K. We have then included the component $\ell=0$ [case JTF(0,1)] and further released the factorization constraint [case JT(0,1)]. It turns out that neither the inclusion of the $\ell=0$ component nor the release of the factorization constraint lead to a sizable decrease of the variational energy or its variance. The same

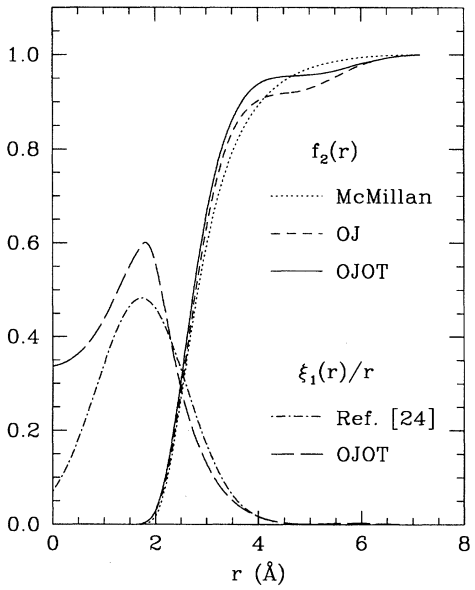

FIG. 2. Two-body correlation function $f_2(r)$ (dots, McMillan; short dashes, optimal Jastrow; solid line, optimal Jastrow + optimal triplet) and triplet factor $\xi_1(r)/r$ (dot-dashed, parametrized triplet from Ref. 24; long dashes, optimal triplet) of ^{4}He at experimental equilibrium density.

holds true for ^{3}He. We conclude that a factorized form with $\ell=1$ and large variational freedom for the function $\xi_1(r)$ is a nearly optimal triplet.

The difference between our best variational energy and the DMC energy is 0.24 K for ^{4}He and 0.20 K for ^{3}He at equilibrium density. This is much larger than the estimated accuracy of $\sim$0.01 K of the optimization procedure. We conclude that this difference is due to n-body correlations, with $n>3$. VMC calculations performed with shadow-type wave functions[20] on ^{4}He strongly indicate the relevance of many-body correlations, particularly at density values close to the freezing. The relevance of four- and five-body correlations were recently investigated in small clusters.[19]

In the following we present the results for the equation of state, the pair distribution function, and the static structure

TABLE I. Energy of ^{4}He (in K) as a function of the density ρ (in Å^{-3}). VMC results are obtained with a wave function containing optimal Jastrow and parametrized triplet correlations (OJT), optimal Jastrow and shadow correlations (OJS), and optimal Jastrow + triplet (OJOT). OJOT-HNC refers to an optimal Jastrow + triplet calculation within the HNC approximation. The exact DMC and GFMC results are also reported.

ρ	0.01964	0.02078	0.02186	0.02401	0.02622	0.02934
OJT[a]	-6.804(15)		-6.862(16)	-6.524(20)	-5.837(23)	
OJS[b]	-6.695(27)		-6.789(23)	-6.615(29)	-6.286(22)	
OJOT	-6.854(2)	-6.915(4)	-6.901(4)	-6.643(3)	-5.991(8)	
OJOT-HNC[c]	-6.51	-6.48	-6.37	-5.90		
DMC	-7.012(2)	-7.111(5)	-7.143(4)	-7.017(6)	-6.557(10)	-5.248(21)
GFMC[d]	-7.034(37)		-7.120(24)	-6.894(48)	-6.564(58)	-5.175(101)

[a]Ref. 5.
[b]Ref. 20.
[c]Ref. 2.
[d]Ref. 13.

TABLE II. Energy E and kinetic energy T (in K) of ^{4}He at the experimental equilibrium density $\rho_{eq}=0.021\ 86$ Å^{-3}. M refers to a VMC calculation with a McMillan wave function (Ref. 24). Other notations as in Table I.

	E	T
M	-5.702(5)	14.712(50)
OJ	-6.001(16)	14.709(20)
OJT[a]	-6.862(16)	
OJOT	-6.901(4)	14.233(8)
DMC	-7.143(4)	14.049(18)

[a]Ref. 5.

function, obtained by using the factorized triplet u_3^F of Eq. (16), with $\ell=1$. For quantities other than the energy, the DMC results that we report are always extrapolated estimators.

A. Liquid ^{4}He

The variational energies are compared in Tables I and II with the exact DMC results and with other variational[5,20] and Green function Monte Carlo[13] calculations. At the equilibrium density, the optimized Jastrow (OJ) wave function improves the energy by 0.3 K over the McMillan form. A further improvement of 0.9 K is obtained including three-body correlations. The remaining difference of 0.24 K from the DMC result is due to higher-order correlations, as previously discussed.

Differences between our results and those of Ref. 5 arise from the fact that a partial optimization was implemented in Ref. 5 whereby the two-body part of the wave function was optimized while keeping a fixed parametrized form of the triplet. Since three-body effects are more important at higher densities, the improvement over the results of Ref. 5 increases with the density. The opposite trend is exhibited by the results of Ref. 20, obtained with a shadow wave function which contains implicitly correlations to all orders. We also note that the discrepancies between our results and those of Ref. 2 are clearly ascribed to higher-order elementary diagrams neglected in the HNC treatment.

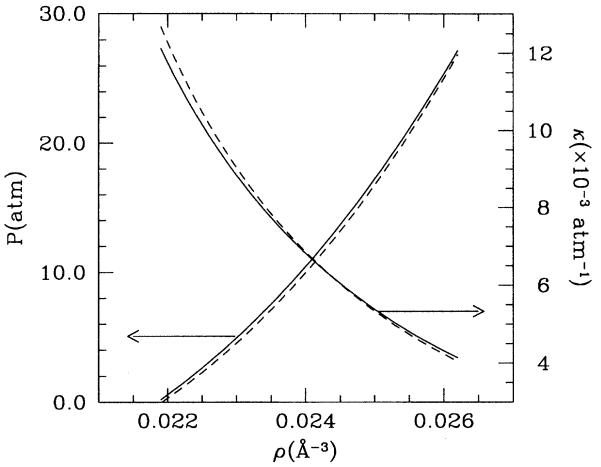

FIG. 4. Pressure P (left scale) and isothermal compressibility κ (right scale) of ^{4}He between equilibrium and freezing density. Solid line, experiment (Ref. 32); dashed line, DMC.

In contrast with the results of Ref. 31 our DMC energies agree with the GFMC results of Ref. 13 at all densities with the exception of $\rho=0.024\ 01$ Å^{-3}, the only one for which the GFMC result does not agree with experimental data. In fact, our energies are very close to the experimental[32] equation of state, as it can be seen from Fig. 3. They are statistically compatible with a polynomial fit of the form $E(\rho)=E_0+B[(\rho-\rho_0)/\rho_0]^2+C[(\rho-\rho_0)/\rho_0]^3$. By χ^2 minimization we get $E_0=-7.144$ K, $B=13.28$ K, $C=9.65$ K, and $\rho_0=0.021\ 92$ Å^{-3}, to be compared to the experimental[32] values of $E_0=-7.14$ K, $B=13.65$ K, $C=7.67$ K, and $\rho_0=0.02185$ Å^{-3}. The resulting pressure $P=\rho^2\partial E/\partial\rho$ and compressibility $\kappa=(1/\rho)\partial\rho/\partial P$ are displayed in Fig. 4. The

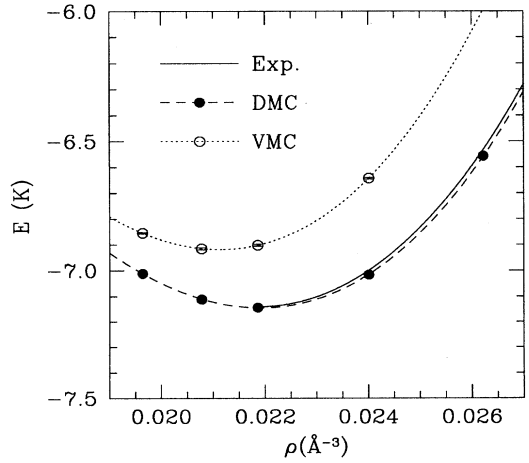

FIG. 3. Equation of state of ^{4}He. Solid circles, DMC; open circles, VMC; solid line, experiment (Ref. 32); the dashed and dotted lines are polynomial fits to the Monte Carlo data.

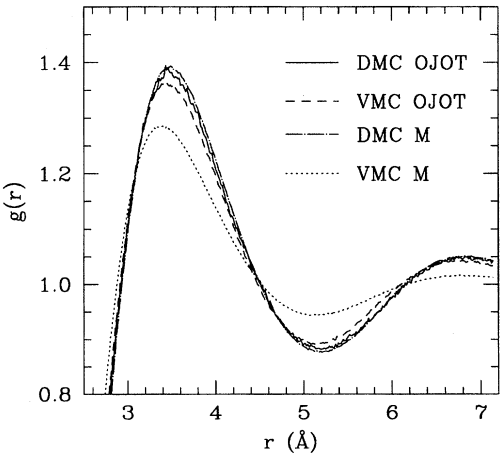

FIG. 5. Pair correlation function $g(r)$ of ^{4}He at equilibrium density. Solid and dashed lines, DMC and VMC results with an optimized OJOT trial function; dash-dotted and dotted lines, DMC and VMC results with a simple McMillan trial function.

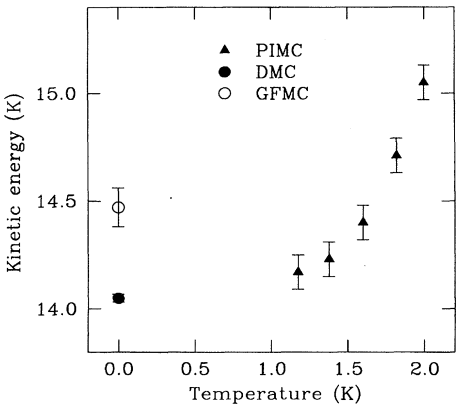

FIG. 6. Ground-state and finite-temperature kinetic energy of ^{4}He at equilibrium density. Solid circle, DMC (this work); open circle, GFMC (Ref. 33); stars, PIMC (Ref. 34).

small discrepancies we find between DMC and experiment are in the opposite direction than reported in Ref. 31 with the HFDHE2 potential.

A good trial wave function provides good energy upper bounds, but also low variance in both VMC and DMC, and reliable extrapolated estimators. The variance we obtain in the case of the optimized Jastrow+Triplet (OJOT) wave function is significantly lower than for other trial wave functions. It ranges from 0.21 at $\rho=0.019\,64$ Å^{-3} to 0.72 at $\rho=0.026\,27$ Å^{-3}. At the equilibrium density $\rho_{\rm eq}=0.021\,86$ Å^{-3} its value 0.34 should be compared with 2.74 of the pure Jastrow of the McMillan form and 1.71 of the OJ wave function. In Fig. 5 we give the pair correlation function

$$g(r)=\frac{1}{N\rho}\sum_{i\neq j}\langle\delta(|\mathbf{r}_i-\mathbf{r}_j-\mathbf{r}|)\rangle \tag{39}$$

at $\rho_{\rm eq}$. Our best estimate for $g(r)$ is shown by the solid line, corresponding to a DMC calculation with the good Ψ_0. One sees the variational $g(r)$ with the OJOT Ψ_0 (dashed line) is very accurate. On the contrary, with a simple McMillan wave function the variational result (dotted line) is far off, and even the DMC result (dash-dotted line) has a sizable bias, the difference between the two DMC results being almost comparable to the difference between VMC and DMC with the good wave function.

An even more striking example is provided by the kinetic energy: At $\rho_{\rm eq}$ (see Table II), we obtain VMC and DMC estimators of 14.7 and 13.3 K with the McMillan wave function, to be compared with 14.23 and 14.05 K calculated with the OJOT wave function. Our best estimate of the kinetic energy, 14.05 K, is somewhat lower than the GFMC result of Ref. 33, and much closer to the zero-temperature extrapolation of the path-integral results of Ceperley and Pollock[34] (see Fig. 6). Table III reports the VMC, DMC, and GFMC (Ref. 33) kinetic energy values at various densities.

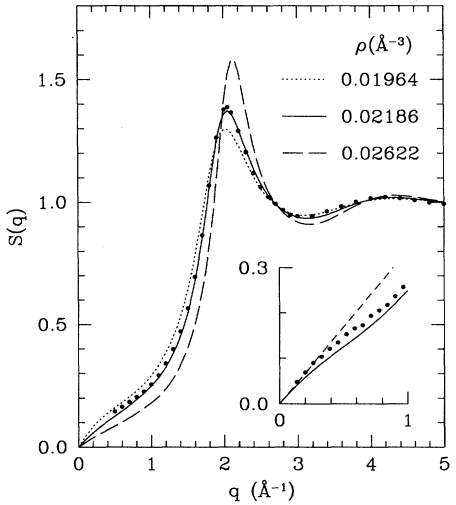

FIG. 7. Static structure factor $S(q)$ of ^{4}He. Dotted, solid, and long-dashed lines are the DMC results at $\rho=0.019\,64$, $0.021\,86$, and $0.026\,22$ Å^{-3}, respectively. The short-dashed line in the inset gives the correct small-q slope for $\rho_{\rm eq}$. The dots are the experimental results at $\rho_{\rm eq}$ of Ref. 35 and of Ref. 36 (in the inset).

Figure 7 displays the static structure factor

$$S(q)=1+\rho\int d\mathbf{r}[g(r)-1]e^{-i\mathbf{q}\cdot\mathbf{r}} \tag{40}$$

at various densities. We also show the neutron scattering data of Svensson *et al.*[35] at equilibrium density. The agreement with experiment is very good, except at very small q. The solid lines are obtained from $g(r)$ by Fourier transform. For $r>L/2$, we assume that $g(r)-1=A[\exp(-Br)\cos(Cr+D)]/r$, with parameters fitted to the calculated $g(r)$ in the range $5<r<L/2$. An independent estimate of $S(q)$ is obtained from the average $N^{-1}\langle\rho_{-\mathbf{q}}\rho_{\mathbf{q}}\rangle$, with $\rho_{\mathbf{q}}=\Sigma_i\exp(-i\mathbf{q}\cdot\mathbf{r}_i)$ and $\mathbf{q}$ a reciprocal lattice vector of the simulation cell. This estimate agrees with the values obtained from Fourier transform down to $q\sim1$ Å^{-1}. For $q\lesssim1$ Å^{-1} we fit a cubic spline to the discrete values at reciprocal lattice vectors in this q range supplemented by the conditions $S(q)=0$, $dS(q)/dq|_{q=0}=\hbar/2Mc$, with the sound velocity c taken from the DMC equation of state.

TABLE III. Kinetic energy of ^{4}He (in K) as a function of the density ρ (in Å^{-3}). Same notations as in Table I.

ρ	0.01964	0.02078	0.02186	0.02401	0.02622
OJOT	11.936(7)	13.069(7)	14.233(8)	16.846(8)	19.639(13)
DMC	11.688(11)	12.881(21)	14.049(18)	16.428(23)	19.312(26)
GFMC[a]	12.08(8)		14.47(9)	17.3(1)	20.1(2)

[a]Ref. 33.

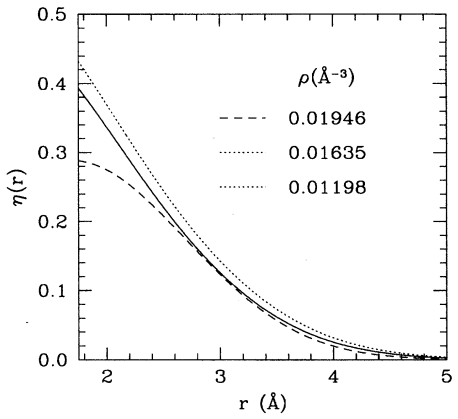

FIG. 8. Backflow correlation function $\eta(r)$ for ^{3}He. Dotted, solid, and dashed lines correspond to ρ=0.011 98, 0.016 35, and 0.019 46 Å^{-3}, respectively.

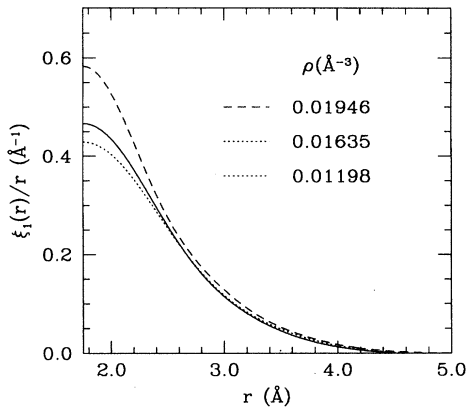

FIG. 10. Triplet correlation function $\xi(r)/r$ for ^{3}He. Dotted, solid, and dashed lines correspond to ρ=0.011 98, 0.016 35, and 0.019 46 Å^{-3}, respectively.

The small q regime is emphasized in the inset of Fig. 7, where the DMC structure factor at equilibrium density is shown along with the small-q x-ray data of Hallock[36] and the correct slope as $q\rightarrow 0$. The discrepancy between the DMC result and experiment in this regime is due to the finite size of the simulation cell, which does not allow the sampling of the zero-point motion of the long-wavelength phonons. Such effect could be included by the procedure described in Ref. 30.

B. Liquid ^{3}He

In the case of ^{3}He, only the bosonic part of the trial wave function can be optimized using the method described in Sec. III C. The backflow correlations in the Slater determinant [see, e.g., Eqs. (11) and (12)] cannot be represented by a simple linear (or quadratic) dependence of $\ln\Psi_0$ on the variational parameters. We used the parametrized form Eq. (12) and optimized its parameters *after* performing a full optimization of F_3 with the backflow parameters fixed as in Ref. 25. All calculations denoted by a B use this *partially* optimized backflow, which is characterized by an $\eta(r)$ having a non-negligible density dependence. In particular, $\eta(r)$ decreases for increasing values of the density, as can be seen in Fig. 8. We also considered the parametrized form used in Ref. 37, which includes a long-range term $1/r^3$ (smoothly cut off at half the simulation cell). Having found no sizable improvement in variational calculation with this addition, all results we present are obtained with the "short-range" backflow of Eq. (12).

In Fig. 9 we show two- and three-body correlations for ^{3}He at equilibrium density for various wave functions. The pair correlation f_2 exhibits the same trend as for ^{4}He, in

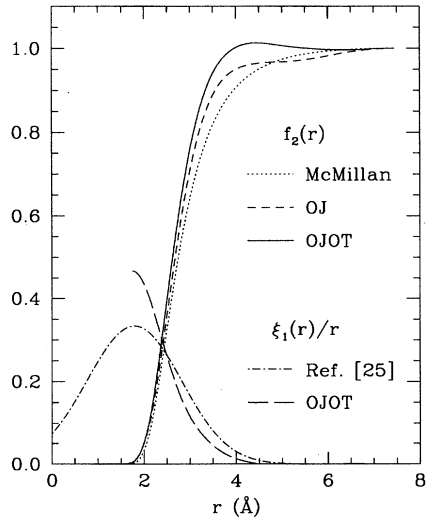

FIG. 9. Two-body correlation function $f(r)$ (dots, McMillan (Ref. 25); short dashes, optimal Jastrow; solid line, optimal Jastrow + optimal triplet) and triplet factor $\xi_1(r)/r$ (dot-dashed, parametrized triplet from Ref. 25; long dashes, optimal triplet) of ^{3}He at the experimental equilibrium density ρ_{eq}=0.016 35 Å^{-3}.

TABLE IV. Energy E and kinetic energy T (in K) of ^{3}He at the experimental equilibrium density ρ_{eq}=0.016 35 Å^{-3}. VMC results are obtained with a McMillan wave function (Ref. 24) (M), optimal Jastrow (OJ), optimal Jastrow and backflow (OBJ), optimal Jastrow + triplet (OJOT), optimal Jastrow, parametrized triplet and backflow (OJTB), and optimal Jastrow + triplet and backflow (OJOTB). The fixed-node DMC result is obtained with the OJOTB trial function. The values reported in square brackets were obtained with an atomic mass of 3.016 a.u., rather that the slightly inaccurate value of 3.000 a.u. that we have used in all the other cases.

	E	T
M	-1.085(34)	12.911(73)
OJ	-1.233(30)	12.920(67)
OJB	-1.659(21)	12.596(57)
OJOT	-1.709(17)	12.606(57)
OJTB	-2.055(15)	12.338(25)
	[-2.123(15)]	[12.270(25)]
OJOTB	-2.095(6)	12.339(8)
	[-2.163(6)]	[12.271(8)]
DMC	-2.299(5)	12.085(35)
	[-2.37(1)]	

TABLE V. Energy of ^{3}He (in K) as a function of the number density (in Å^{-3}). OJOTB refers to the VMC result with a wave function with optimized Jastrow and triplet, and a partially optimized backflow. The fixed-node DMC results are obtained with the same trial function.

ρ	0.01198	0.01413	0.01635	0.01797	0.01946
OJOTB	-1.917(3)	-2.099(3)	-2.095(6)	-1.920(6)	-1.617(6)
DMC	-2.000(2)	-2.258(4)	-2.299(5)	-2.187(5)	-2.006(7)

going from the McMillan wave function to the optimal Jastrow+triplet (and backflow). However, the shoulder at $r\sim 4$ Å is higher in ^{3}He, and exceeds 1 in the OJOT wave function. The optimal triplet correlation $\xi(r)$ also shows the same trend as in ^{4}He, being higher than the parametrized form of Ref. 25 at $r\sim 2$ Å, and decreasing faster at large r. However, it has an appreciable density dependence at variance with the case of ^{4}He and it is shown in Fig. 10. This may be tentatively attributed to an interplay between triplet and backflow correlations in ^{3}He.

The variational energies for various wave functions and densities are compared in Tables IV and V, with the DMC fixed-node results. At the equilibrium density, the optimization of $u_2(r)$ in a Jastrow wave function with plane waves determinants improves the energy by only 0.15 K over the McMillan form. Including triplet and backflow we obtain a further improvement of 0.86 K. The remaining difference of 0.20 K from the DMC result is due to higher-order correlation. The VMC and DMC equations of state are compared in Fig. 11. Like in ^{4}He, the difference between the two predictions increases with density, as higher-order correlations become more important. The effect of the fixed-node approximation clearly shows up in the sizable discrepancy between DMC the result and the experimental[38] equation of state. Total and kinetic energy values as function of the density are reported in Tables V and VI.

There is a discrepancy between our fixed-node DMC results for the total energy and the fixed-node GFMC results of Ref. 37 obtained with the same number of particles. At equilibrium density, for instance, Ref. 37 quotes a value of $-2.37(1)$ K, to be compared with our result of

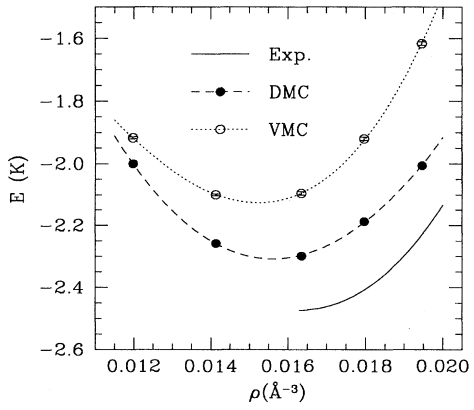

FIG. 11. Equation of state of ^{3}He. Solid circles, DMC; open circles, VMC; solid line, experiment (Ref. 38); the dashed and dotted lines are polynomial fits to the Monte Carlo data.

TABLE VI. Kinetic energy of ^{3}He (in K) as a function of the number density (in Å^{-3}). The fixed-node DMC results are obtained with the same trial function. Notations as in Table V.

ρ	0.01198	0.01413	0.01635	0.01797	0.01946
OJOTB	8.131(7)	9.982(9)	12.339(8)	14.193(12)	16.020(12)
DMC	7.951(19)	9.825(21)	12.085(35)	13.833(31)	15.450(21)

$-2.299(5)$. The difference is to be attributed to the slightly inaccurate value we used for the mass of the ^{3}He atom, namely, $m=3$ a.u. We have verified that with the correct value of the mass ($m=3.016$ a.u.) the DMC energy decreases by 0.07(1) K, which brings our result in agreement with Ref. 37, and reduces the discrepancy with the experiment to about 0.1 K. The inaccurate value of the mass also biases our VMC results. In this case the correction can be inferred directly from the kinetic energy, and amounts to a decrease of -0.068 K at equilibrium density. The correction brings into agreement the variational energy of $-2.055(15)$ of our OJTB wave function (see Table IV for notation), with the value of $-2.13(2)$ obtained in Ref. 37 using a presumably equivalent wave function (parametrized triplet and backflow, and optimal Jastrow correlation). Finally we note that the same correction would shift the energy of our OJOTB wave function down to $-2.163(6)$ K, the best variational upper bound to date.

Figure 12 displays the static structure function at various densities. For the experimental density, we show also the experimental x-ray result of Achter and Meyer.[39] Again we note that the fixed-node approximation results in appreciable differences between the DMC prediction and the experiment. Thus we do not perform any small-q fit to the correct linear behavior in this case, at variance with ^{4}He.

In calculating pair correlations we have also resolved the spin components

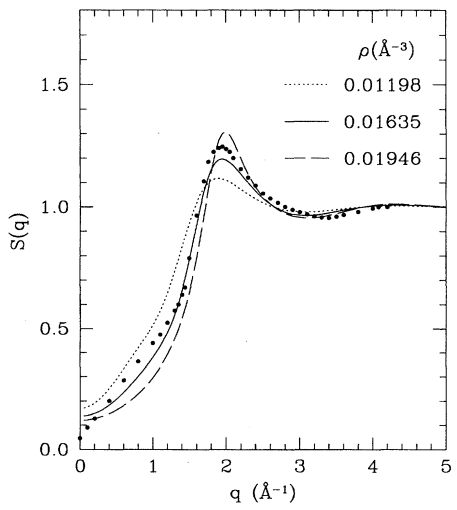

FIG. 12. Static structure factor $S(q)$ of ^{3}He. Dotted, solid, and long-dashed lines are the DMC results at ρ=0.011 98, 0.016 35, and 0.019 46 Å^{-3}, respectively. The dots are the experimental results at ρ_{eq} of Ref. 39.

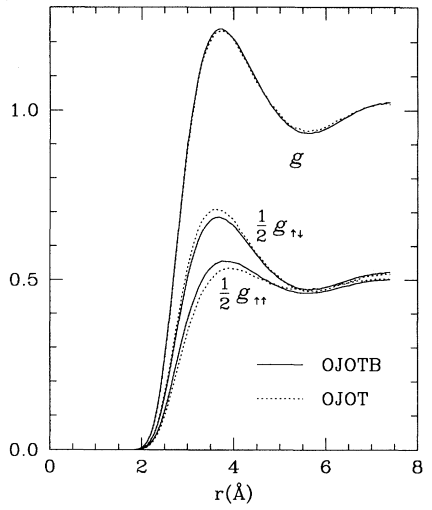

FIG. 13. Total pair correlation function $g(r)$ and spin-resolved pair correlations $g_{\uparrow\uparrow}$ and $g_{\uparrow\downarrow}$ for ^{3}He at equilibrium density. Solid and dotted lines correspond to DMC calculations with an optimized trial function with backflow (OJOTB) and without backflow (OJOT), respectively.

$$g_{\uparrow\uparrow}(r)=\frac{4}{N\rho}\sum_{i\neq j=1}^{N/2}\langle\delta(|\mathbf{r}_i-\mathbf{r}_j-\mathbf{r})|\rangle \tag{41}$$

and

$$g_{\uparrow\downarrow}(r)=\frac{4}{N\rho}\sum_{i=1}^{N/2}\sum_{j=N/2+1}^{N}\langle\delta(|\mathbf{r}_i-\mathbf{r}_j-\mathbf{r})|\rangle, \tag{42}$$

where particles 1 to $N/2$ have spin up, particles $N/2+1$ to N have spin down, and $g(r)=(1/2)[g_{\uparrow\uparrow}(r)+g_{\uparrow\downarrow}(r)]$.

In Fig. 13 we show the extrapolated DMC pair correlations obtained with two trial functions with different nodes, namely the optimized form with or without backflow (OJOTB and OJOT, respectively). The difference is seen to be very small on $g(r)$, but appreciable on the spin-resolved components. Backflow considerably reduces the difference $g_{\uparrow\downarrow}-g_{\uparrow\uparrow}$ (for instance, by 29% at the peak of $g_{\uparrow\downarrow}$), pointing to a weaker tendency towards short-range antiferromagnetic order. This result deserves further investigation, as the quantity being considered is dependent on the nodal structure, and backflow nodes are not perfect, as shown by comparison with the experimental structure and equation of state.

VI. CONCLUSIONS

In this paper we have presented an optimization procedure for Jastrow and triplet correlation based upon Monte Carlo calculations. Both the pair and the triplet correlations have been expanded in terms of suitable basis functions, and the expansion coefficients were treated as variational parameters. The number of basis functions considered has been taken large enough to ensure a full optimization. This method improves upon previously developed Euler equation procedures, based on HNC or FHNC theory or limited to the pair correlation function. We found that possible corrections to the Feynman ansatz for the triplet correlation are almost negligible and that the structure of the pair correlation at intermediate range is significantly influenced by triplet correlations.

The EMC method provides the best variational results ever obtained for the equation of state of both liquid ^{4}He and ^{3}He, with significant improvements of the energy upper-bounds at the higher densities. The optimized wave functions found by using the EMC method have been used in DMC calculations for the Bose system and fixed-node DMC for the Fermi system, yielding accurate results for the total energy, kinetic energy, pair distribution, and static structure function. Results for the momentum distribution and the one-body density matrix will be given elsewhere.[40]

The sizable discrepancies still present between variational and DMC energies, after triplet optimization, point unambiguously to the importance of n-body correlations, with $n>3$, particularly at high densities.

We have observed an appreciable dependence of the spin correlation on the nodes, pointing to a suppression of short-range antiferromagnetic order when better nodes are used. This agrees with the general tendency of correlation in reducing the importance of magnetic effects predicted by mean field. We also note that the refinement of variational wave functions that we have accomplished here might be useful for calculations of excitations from the ground state, along the line pursued by Kwon *et al.*[41] in the two-dimensional electron gas.

ACKNOWLEDGMENT

Most of this work was carried out using computing facilities of CNUCE, an institute supported by CNR and MURST.

[1] L. J. Lantto and P. J. Siemens, Phys. Lett. **68B**, 308 (1977); L. J. Lantto, A. D. Jackson, and P. J. Siemens, *ibid.* **68B**, 311 (1977).
[2] E. Krotscheck, Phys. Rev. B **33**, 3158 (1986).
[3] Q. N. Usmani, S. Fantoni, and V. R. Pandharipande, Phys. Rev. B **26**, 6123 (1982).
[4] E. Manousakis, S. Fantoni, V. R. Pandharipande, and Q. N. Usmani, Phys. Rev. B **28**, 3770 (1983).
[5] S. A. Vitiello and K. E. Schmidt, Phys. Rev. B **46**, 5442 (1992).
[6] D. M. Ceperley and M. H. Kalos, in *Monte Carlo Methods in Statistical Physics*, edited by K. Binder (Springer, New York, 1979).
[7] G. V. Chester and L. Reatto, Phys. Rev. **155**, 88 (1967).
[8] R. A. Smith, A. Kallio, M. Puoskari, and P. Toropainen, Nucl. Phys. **A328**, 186 (1979).
[9] E. Feenberg, *Theory of Quantum Liquids* (Academic, New York, 1969).
[10] J. W. Clark, Nucl. Phys. **A328**, 587 (1979).
[11] C. E. Campbell, Phys. Lett. **44A**, 471 (1973); C. C. Chang and C.

E. Campbell, Phys. Rev. B **15**, 4328 (1977).
[12] V. R. Pandharipande, Nucl. Phys. **A181**, 33 (1972); **A178**, 123 (1971); **A174**, 641 (1971).
[13] M. H. Kalos, M. A. Lee, P. A. Whitlock, and G. V. Chester, Phys. Rev. B **24**, 115 (1981).
[14] P. J. Reynolds, D. M. Ceperley, B. J. Alder, and W. A. Lester, J. Chem. Phys. **77**, 5593 (1982).
[15] D. M. Ceperley, in *Recent Progress in Many-Body Theories*, edited by J. Zabolitzky (Springer, New York, 1981); J. Stat. Phys. **63**, 1237 (1991).
[16] D. M. Ceperley, G. V. Chester, and M. H. Kalos, Phys. Rev. D **13**, 3208 (1976).
[17] C. M. Umrigar, K. G. Wilson, and J. W. Wilkins, Phys. Rev. Lett. **60**, 1719 (1988); C. M. Umrigar, K. G. Wilson, and J. W. Wilkins, in *Computer Simulation Studies in Condensed Matter Physics*, edited by D. P. Landau, K. K. Mon, and H. B. Schüttler (Springer, Berlin, 1988), p. 185.
[18] D. M. Ceperley (unpublished).
[19] A. Mushinski and M. P. Nightingale, J. Chem. Phys. **101**, 8831 (1994).
[20] T. McFarland, S. A. Vitiello, L. Reatto, G. V. Chester, and M. H. Kalos, Phys. Rev. B **50**, 13577 (1994).
[21] S. Moroni, S. Fantoni, and G. Senatore, Europhys. Lett. **30**, 93 (1995).
[22] R. A. Aziz, V. P. S. Nain, J. S. Carley, W. L. Taylor, and G. T. Conville, J. Chem. Phys. **70**, 4330 (1979).
[23] D. M. Ceperley, G. V. Chester, and M. H. Kalos, Phys. Rev. B **16**, 3081 (1977).
[24] K. E. Schmidt, M. W. Kalos, M. A. Lee, and G. V. Chester, Phys. Rev. Lett. **45**, 573(1980).
[25] K. E. Schmidt, M. A. Lee, M. W. Kalos, and G. V. Chester, Phys. Rev. Lett. **47**, 807 (1981).
[26] Y. Kwon, D. M. Ceperley, and R. M. Martin, Phys. Rev. B **48**, 12037 (1993).
[27] W. H. Press, S. A. Teukolsky, W. T. Vetterling, and B. P. F. Flannery, *Numerical Recipes* (Cambridge University Press, Cambridge, England, 1992).
[28] C. J. Umrigar, M. P. Nightingale, and K. J. Runge, J. Chem. Phys. **99**, 2865 (1993).
[29] K. S. Liu, M. H. Kalos, and G. V. Chester, Phys. Rev. A **10**, 313 (1974).
[30] P. A. Whitlock, D. M. Ceperley, G. V. Chester, and M. H. Kalos, Phys. Rev. B **19**, 5598 (1979).
[31] J. Boronat and J. Casulleras, Phys. Rev. B **49**, 8920 (1994).
[32] P. R. Roach, J. B. Ketterson, and Chia-Wei Woo, Phys. Rev. A **2**, 543 (1970).
[33] P. A. Whitlock and R. M. Panoff, Can. J. Phys. **65**, 1409 (1987).
[34] D. M. Ceperley and E. L. Pollock, Phys. Rev. Lett. **56**, 351 (1986).
[35] E. C. Svensson, V. F. Sears, A. D. B. Woods, and P. Martel, Phys. Rev. B **21**, 3638 (1980).
[36] R. B. Hallock, Phys. Rev. A **5**, 320 (1972).
[37] R. M. Panoff and J. Carlson, Phys. Rev. Lett. **62**, 1130 (1989).
[38] T. R. Roberts, R. H. Sherman, and S. G. Sydoriak, J. Res. Natl. Bur. Stand. A **68**, 567 (1964); R. A. Aziz and R. K. Pathria, Phys. Rev. A **7**, 809 (1972).
[39] E. K. Achter and L. Meyer, Phys. Rev. **188**, 291 (1969).
[40] S. Moroni, S. Fantoni, and G. Senatore (unpublished).
[41] Y. Kwon, D. M. Ceperley, and R. M. Martin, Phys. Rev. B **50**, 1684 (1994).